Kinked-Helices Model of the Nicotinic Acetylcholine Receptor Ion Channel and Its Complexes with Blockers: Simulation by the Monte Carlo Minimization Method

Denis B. Tikhonov and Boris S. Zhorov
Sechenov Institute of Evolutionary Physiology and Biochemistry, Russian Academy of Sciences, St. Petersburg, Russia

ABSTRACT A model of the nicotinic acetylcholine receptor ion channel was elaborated based on the data from electron microscopy, affinity labeling, cysteine scanning, mutagenesis studies, and channel blockade. A restrained Monte Carlo minimization method was used for the calculations. Five identical M2 segments (the sequence EKMTLSISVL^{10}LALTVFLLVI^{20}V) were arranged in five-helix bundles with various geometrical profiles of the pore. For each bundle, energy profiles for chlorpromazine, QX-222, pentamethonium, and other blocking drugs pulled through the pore were calculated. An optimal model obtained allows all of the blockers free access to the pore, but retards them at the rings of residues known to contribute to the corresponding binding sites. In this model, M2 helices are necessarily kinked. They come into contact with each other at the cytoplasmic end but diverge at the synaptic end, where N-termini of M1 segments may contribute to the pore. The kinks disengage α-helical H-bonds between Ala^{12} and Ser^{8}. The uncoupled lone electron pairs of Ser^{8} carbonyl oxygens protrude into the pore, forming a hydrophilic ring that may be important for the permeation of cations. A split network of H-bonds provides a flexibility to the chains Val^{9}-Ala^{12}, the numerous conformations of which form only two or three intrasegment H-bonds. The cross-ectional dimensions of the interface between the flexible chains vary essentially at the level of Leu^{11}. We suggest that conformational transitions in the chains Val^{9}-Ala^{12} are responsible for the channel gating, whereas rotations of more stable α-helical parts of M2 segments may be necessary to transfer the channel in the desensitized state.

INTRODUCTION

Nicotinic acetylcholine receptors (nAChRs) are ligand-gated ion channels involved in signal transduction in interneuron and neuromuscular junctions (Devillers-Thiery et al., 1993; Galzi and Changeux, 1994). They incorporate five subunits, each subunit having a large extracellular domain at the N end and four transmembrane segments, M1–M4. Mutagenesis and physiological studies indicate that the pore is lined by M2 segments (M2s) from each of the five subunits (Changeux et al., 1992; Galzi and Changeux, 1995). Solid-state NMR spectroscopy demonstrated α-helical conformation and transmembrane orientation of M2 peptide (Bechinger et al., 1991). Fourier transform infrared spectroscopy of the purified nAChR reconstructed into lipid vesicles indicated predominantly α-helical structure of the receptor transmembrane domains (Baenziger and Methot, 1995). Synthetic channels composed of four or five M2s exhibit some electrophysiological and pharmacological properties of nAChRs (Oblatt-Montal et al., 1993a,b). Periodicity of the residues responsible for the channel functions (Table 1) suggests an α-helical structure for M2s that form a five-helix bundle (see Hille, 1992, for a review). The bundle is believed to have a funnel-like shape with a narrow cytoplasmic end, and six rings of homologous residues facing the pore at the levels of Glu^{1} (intermediate ring), Thr^{4} (threonine ring), Ser^{8} (serine ring), Leu^{11} (equatorial ring), Val^{15} (valine ring), and Leu^{18} (outer leucine ring). The five-helix bundle was visualized in structural models of nAChR pore (Oiki et al., 1988, 1990; Furois-Corbin and Pullman, 1989; Eisenman et al., 1990; von Kitzing, 1995). The structure of other transmembrane segments remains unknown; β-sheets may be present in some of them (Hucho et al., 1994). N-termini of M1s may contribute to the synaptic end of the pore (Akabas and Karlin, 1995; DiPaola et al., 1990); the data support the funnel-like model of the channel. Assuming a 3-D homology of nAChR with the heat-labile enterotoxin, Ortels and Lunt (1996) proposed a model of nAChR with a central pore composed of slightly bent α-helical M2s and β-strands dominating in the remainder of the structure.

Electron microscopy studies suggest that M2s are kinked approximately in their midpoints (Unwin, 1993, 1995, 1996). The rotation of the kinked helices was suggested to cause a transition between the open and the closed states of the channel (Unwin, 1995). Using the electron microscopy data, Sankararamakrishnan et al. (1996) created models of the open and the closed channel with the kinked helices. The open-channel model predicts the minimum diameter of the pore to be 12 Å, the value conflicting with the data on permeability of the channel for organic cations (Dwyer et al., 1980; Nutter and Adams, 1995). To explain this disagreement, the authors of the model suggested that water molecules bound to the channel walls would narrow the pore. A network of H-bonds between the hydrophilic residues of the channel and the intrapore waters could be stable

Received for publication 7 July 1997 and in final form 17 October 1997.
Address reprint requests to Dr. Boris S. Zhorov, Department of Biochemistry, McMaster University, 1200 Main Street West, Hamilton, ON L8N 3Z5, Canada. Tel.: 905-525-9140, ext. 22864; Fax: 905-522-9033; E-mail: zhorov@nfss.iephb.ru.

0006-3495/98/01/242/14 $2.00

TABLE 1 Aligned sequences of M2 segments in nAChRs

	Position[#]																				
M2 segment	**1***	2	3	**4***	5	6	7	**8***	9	10	**11***	**12***	13	14	**15***	16	17	**18***	**19***	20	21
Consensus	E	K	M	T	L	S	I	S	V	L	L	A	L	T	V	F	L	L	V	I	V
α *Torpedo*	E	K	M	T	L	S	I	S	V	L	L	S	L	T	V	F	L	L	V	I	V
β *Torpedo*	E	K	M	S	L	S	I	S	A	L	L	A	V	T	V	F	L	L	L	L	A
γ *Torpedo*	Q	K	C	T	L	S	I	S	V	L	L	A	Q	T	I	F	L	F	L	I	A
δ *Torpedo*	E	K	M	S	T	A	I	S	V	L	L	A	Q	A	V	F	L	L	L	T	S
α mouse	E	K	M	T	L	S	I	S	V	L	L	S	L	T	V	F	L	L	V	I	V
β mouse	E	K	M	G	L	S	I	F	A	L	L	T	L	T	V	F	L	L	L	L	A
γ mouse	Q	K	C	T	V	A	T	N	V	L	L	A	Q	T	V	F	L	F	L	V	A
δ mouse	E	K	T	S	V	A	I	S	V	L	L	A	Q	S	V	F	L	L	L	I	S
α3 rat	E	K	V	T	L	C	I	S	V	L	L	S	L	T	V	F	L	L	V	I	T
α4 rat	E	K	V	T	L	C	I	S	V	L	L	S	L	T	V	F	L	L	L	I	T
β2 rat	E	K	M	T	L	C	I	S	V	L	L	A	L	T	V	F	L	L	L	I	S
α2 chicken	E	K	I	T	L	C	I	S	V	L	L	S	L	T	V	F	L	L	L	I	T
α3 chicken	E	K	V	T	L	C	I	S	V	L	L	S	L	T	V	F	L	L	V	I	T
α4 chicken	E	K	I	T	L	C	I	S	V	L	L	S	L	T	V	F	L	L	L	I	T
α7 chicken	E	K	I	S	L	G	I	T	V	L	L	S	L	T	V	F	M	L	L	V	A
Open channel	C			C				C			C	C			C			C			
Closed channel	C			C	C			C		C	C	C			C			C			

Positions corresponding to the residues that face the pore in the present model are marked by *. Residues labeled by chlorpromazine (Revah et al., 1990) are underlined. Residues affecting QX-222 binding (Charnet et al., 1990) are double underlined. Positions of cysteine mutants that are labeled by sulfhydryl reagents in the open and closed states (Akabas et al., 1994; Akabas and Karlin, 1995) are marked by C.

[#] Position i in the numbering scheme used in this work corresponds to position $i - 2$ in an alternative numbering scheme (Lester, 1992).

enough to diminish the effective diameter of the pore for transient penetrating cations. However, the water molecules may be displaced by amphiphilic ligands whose dwelling time inside the pore reaches tens of milliseconds. The well-known noncompetitive blockers of nAChR are rather small to bind tightly in the pore of 12 Å in diameter. In the absence of a high-resolution structure of nAChR, the actual diameter of the pore remains unknown. On the other hand, the recently resolved crystal structure of the five-helix bundle in the cartilage oligomeric matrix protein, a possible prototype ion channel, presents an example of a narrow pore (Malashkevich et al., 1996).

The suggestion on the channel gating via rotations of entire M2s does not agree with the cysteine-scanning data that both open and closed states of nAChR allow sulfhydryl reagents to reach nearly the same residues in M2s (Akabas et al., 1994; Akabas and Karlin, 1995). Dimensions of the pore and the gate should correlate: essential conformational changes (e.g., rotations of entire M2s) are necessary to close a wide pore, whereas even a slight rearrangement of hydrophobic residues at a channel constriction comparable in dimensions with a hydrated cation may block the permeation (Zhorov and Ananthanarayanan, 1996). Further modeling studies are necessary to explain seemingly conflicting data from various approaches.

A sensitive touchstone for models of nAChR pore is their ability to explain structure-activity relationships of noncompetitive blockers. The pore of nAChR is blocked by various organic cations: chlorpromazine (Benoit and Changeux, 1993), local anesthetics QX-222 and QX-314 (Neher and Steinbach, 1978), procaine (Adams, 1977), triphenylmethylphosphonium (Hucho et al., 1986), tubocurarine (Large and Sim, 1986), phencyclidine (Aguayo and Albuquerque, 1986; Papke and Oswald, 1989), bis-ammonium compounds (Zhorov et al., 1991; Antonov et al., 1995), MK-801 (Amador and Dani, 1991), etc. The binding sites for chlorpromazine (Revah et al., 1990) and triphenylmethylphosphonium (Hucho et al., 1986) were determined by the affinity labeling method. The mutation experiments determined residues responsible for the binding of QX-222 (Leonard et al., 1988; Charnet et al., 1990). The data on the channel blockade were used by Furois-Corbin and Pullman (1989) to create a funnel-like model of nAChR that allows chlorpromazine (CPZ) to pass the bulky Leu^{18} and Val^{15} rings and reach the Ser^{8} ring. An analysis of conformation-activity relationships of bis-ammonium blockers of the neuronal and muscle nAChRs had led us to predict dimensions of the pore at Ser^{8} and Thr^{4} rings (Zhorov et al., 1991; Brovtsyna et al., 1996; Tikhonov et al., 1996). In the present work, we employed the restrained Monte Carlo minimization method to create several five-helix-bundle models of nAChR with various geometrical profiles of the pore. We further simulated docking of structurally different blockers in the bundles to select an optimal model that predicts the binding sites of the blockers in agreement with the experimental data. The optimal model obtained is consistent with the available data on the permeation of organic cations, affinity labeling, cysteine scanning, and mutagenesis experiments. This model also agrees with some (but not all) suggestions of Unwin (1993, 1995) deduced from the electron microscopy images of nAChR.

METHOD

The protocol of the Monte Carlo minimization method (MCM) (Li and Scheraga, 1988) and an ECEPP/2 force field (Momany et al., 1975; Nemethy et al., 1983) were used to search for optimal conformations. Energy was minimized in the space of generalized coordinates (Zhorov, 1981, 1983): torsions of M2s and blockers, bond angles of blockers, positions of M2s and blockers (Cartesian coordinates of their root atoms), and orientations of M2s and blockers (Euler angles of the local coordinate systems centred at the root atoms). Calculations were carried out with a ZMM program package (Zhorov, 1981, 1993). Geometrical profiles of the pore and positions of the blockers along the pore were restrained with flat-bottom penalty functions (Brooks et al., 1985) with a bottom width of 1 Å. Initial assembly of the models, their visualization, and manipulation were performed with a molecular graphics program elaborated by one of us (Tikhonov, to be published).

Trajectories were calculated at $T = 600$ K. A subsequent starting point in a trajectory was obtained by changing a randomly selected generalized coordinate (excluding bond angles) of the preceding point by a random increment. From a given starting point, energy was minimized in the space of all generalized coordinates until the norm of energy gradient became less than 1 kcal·mol^{-1}·rad^{-1}. The resulting minimum-energy conformation (MEC) was accepted in the trajectory if its energy (E) was less than that of the preceding point of the trajectory (E_p) or if a random number $n \in (0, 1)$ was less than $\exp(-(E - E_p)/RT)$. MCM trajectories were terminated when the last N_u energy minimizations did not lower the energy of the best MEC found. In different experiments, the parameter N_u varied between 100 and 3000 (see results).

Atom-atom interactions were calculated with a cutoff distance of 7.5 Å. The partial charges at the atoms of blocking molecules were calculated by the CNDO/2 method. The lowest-energy MECs of lone blockers were used as starting approximations for the docking of the blockers in the five-helix bundle. During the docking, the main-chain torsions and positions of M2s, as well as bond angles and rings of the blockers, were kept rigid, and the other generalized coordinates were varied. Minimum dimensions of the blockers that may correspond to the cross-sectional dimensions of the pore at their binding sites were calculated, taking into account van der Waals radii of atoms (Zhorov et al., 1991). Other details of the calculations are described elsewhere (Zhorov and Ananthanarayanan, 1996).

RESULTS AND DISCUSSION

General assumptions

α-Helical M2s are believed to be the major pore-lining segments in nAChRs (Unwin, 1995; Galzi and Changeux, 1995; Bertrand et al., 1993), whereas N-end parts of M1s contribute to the pore only partially (DiPaola et al., 1990; Akabas and Karlin, 1995). We composed the pore of M2s only. Because M2s are conserved in various nAChRs (Le Novere and Changeux, 1995), we used a consensus sequence (Table 1) that would corresponds to the Ser^{12} to Ala^{12} mutant of the M2 segment from the α-subunit of *Torpedo californica* nAChR. Nicotinic acetylcholine receptors from different sources have diverse permeabilities and sensitivities to blockers (Sands and Barish, 1991; Vernino et al., 1992; Zhorov et al., 1991; Cuevas and Adams, 1994). However, many compounds (e.g., bisammonium blockers) demonstrate analogous tendencies of structure-activity relationships in muscular and neuronal nAChRs (Brovtsyna et al., 1996; Tikhonov et al., 1996). This justifies our use of the consensus M2 for a general model of nAChR pore.

Helices between Thr^4 and Ser^8 are not tilted radially to the pore axis

First we studied conformational properties of the single M2. The α-helical structure was biased by restraining H-bonds $NH_i \cdots O_{i-4}$ in the range of 1.7–2.0 Å. Conformations of the side chains were MCM-optimized ($N_u = 500$), their starting torsions being as in the optimal α-helical conformations of the corresponding monopeptides. The latter were calculated earlier (Zhorov, unpublished data) with the ZMM program and were found to coincide with those reported by Vasques et al. (1983). During the search, only side-chain torsions were randomized, but all of the torsions were varied in energy minimizations.

The optimal MEC found is a linear α-helix with Ser^8 and Thr^4 hydroxyls H-bonding to the main-chain carbonyls of Ser^4 and Glu^1, respectively. Ser^8 and Thr^4 side chains are known to face the pore. In these residues, O^γ_Ser^8 and H-C^γ_Thr^4 are the atoms farthest from the helix axis (3.9 and 5.3 Å, respectively). Hence, in the five-helix bundle, the Ser^8 ring would be wider than the Thr^4 ring, even if the helical axes between Ser^8 and Thr^4 were not tilted radially to the pore axis. Various experimental and theoretical data indicate that the Ser^8 ring is indeed wider than the Thr^4 ring. The latter forms the narrowest constriction in the open channel (Hucho and Hilgenfeld, 1989; Villarroel et al., 1991; Villarroel and Sakmann, 1992). A Thr^4 to Ser^4 mutation increases the channel permeability, probably because of an enlargement of the pore (Imoto et al., 1991). Electron microscopy images of the open channel (Unwin, 1995) and the model by Sankararamakrishnan et al. (1996) suggest that the Thr^4 ring is narrower than the Ser^4 ring. In the series of biscationic blockers $N(Et)_3$-$(CH_2)_5$-$NR^1R^2R^3$, the compounds with quaternary ammonium groups $NR^1R^2R^3$ are more active than the compounds of similar dimensions with tertiary or secondary amino groups (Brovtsyna et al., 1996). The smaller cationic head of these blockers supposedly binds to the Thr^4 ring. The low activity of the blockers with the tertiary/secondary amino group indicates that the latter does not form H-bonds with Thr^4 oxygens, implying that the CH_3_Thr^4 rather than the HO_Thr^4 group protrudes into the

pore. The predicted dimensions of the pore at Ser^8 and Thr^4 rings are, respectively, 6.1 × 8.3 Å and 5.5 × 6.4 Å (Zhorov et al., 1991; Brovtsyna et al., 1996). The different dimensions of the Ser^8 and Thr^4 rings correlate with the nonequal protrusions of these residues into the pore, suggesting that the helices between the two rings do not have a significant radial slope to the pore axis.

A kinked-helices bundle would allow blockers to fit the Ser^8 ring

CPZ labels Thr^4 at the γ-subunit and Ser^8 at all of the subunits of *T. californica* nAChR (Revah et al., 1990). The fact that CPZ reaches the Ser^8 ring indicates that the Leu^{11}/Ala^{12} ring may accommodate the tricyclic moiety of CPZ, the minimum profile dimensions of which are 5.7 × 12.2 Å. The fact that the Leu^{11}/Ala^{12} ring is much wider than the Ser^8 ring (6.1 × 8.3 Å) means that the helical axes between Leu^{11}/Ala^{12} and Ser^8 are radially tilted to the pore axis. The tilt between Leu^{11}/Ala^{12} and Ser^8 and the absence of the tilt between Ser^8 and Thr^4 means that M2 helices are kinked between Ser^8 and Leu^{11}/Ala^{12}. This agrees with the suggestion of Unwin (1993, 1995) that M2s are kinked near the Leu^{11} ring. The results of cysteine scanning (Akabas et al., 1994) also imply a kink near Leu^{11}: in the closed channel, positions 10, 11, and 12 are accessible to sulfhydryl reagents (Table 1), which is inconsistent with the helical structure.

Similar considerations that CPZ has to pass the rings of the bulky Val^{15} and Leu^{18} residues to reach a narrow Ser^8 ring had led Furois-Corbin and Pullman (1989) to a funnel-like model of nAChR composed of straight (not kinked) helices. Given the dimensions of the Thr^4 ring (5.5 × 6.4 Å) and the Leu^{11}/Ala^{12} ring (at least 5.7 × 12.2 Å), the dimensions of the Ser^8 ring in the straight-helices bundle would exceed 6.1 × 8.3 Å. Mutations of Ser^8 affect the pore blockade by QX-222 (Charnet et al., 1990), suggesting that these residues contribute to the binding site of QX-222. The minimum profile dimensions of QX-222 (6.0 × 8.6 Å) are close to the predicted dimensions of the Ser^8 ring (6.1 × 8.3 Å). In the model by Furois-Corbin and Pullman (1989), the side chains of Ser^8 residues extend into the pore. In our model, side chains of Ser^8 do not protrude into the pore, but are folded to form H-bonds with the main-chain carbonyls (Fig. 1 *e*). To retard QX-222 and bis-ammonium compounds at the Ser^8 ring, the helical axes of M2s with the folded Ser^8 side chains should be even closer to the pore axis than the helices with the extended Ser^8 side chains. The bundle of the tilted but straight M2s does not render the Ser^8 ring constricted enough to retard QX-222 and bis-ammonium compounds. In other words, the data on ligand binding suggest the dimensions of Thr^4, Ser^8, and Leu^{11}/Ala^{12} rings to be 5.5 × 6.4 Å, 6.1 × 8.3 Å, and at least 5.7 × 12.2 Å, respectively. A model composed of the straight helices would not satisfy all the three requirements simultaneously. These are the "pharmacological" reasons for the kinked M2s.

Kinked-helix conformations of the lone M2 correspond to local energy minima

It is well known that an α-helix may be terminated or kinked because of H-bonds between Ser/Thr side chains and the main-chain carbonyls in the preceding helical turn (Levitt, 1978; Bolin et al., 1982). To test whether such H-bonds would stabilize kinks in the isolated α-helix, we carried out MCM calculations of the entire M2 and its undecapeptide models $(Ala)_4$-X-$(Ala)_4$, where X = Ile-Ser-Val and X = Leu-Thr-Leu. Both main-chain and side-chain torsions were randomized in these calculations. Relatively short MCM trajectories (N_u = 500) starting from the ideal α-helical conformations yielded many MECs with various kinks, and Ser and Thr side chains H-bonding to the main-chain carbonyls. Similar MCM calculations of the undecapeptides with X = Ile-Ala-Val and X = Leu-Leu-Leu did not yield kinks. A longer MCM trajectory of M2 (N_u = 3000) yielded many MECs within 7 kcal/mol of the apparent global minimum, with Ser and Thr side chains H-bonding to the main-chain carbonyls. None of these MECs were kinked in the middle of the helix, but many MECs were kinked at the helical ends. Thus the linear helices are more stable than the kinked ones, implying that the kinks are not an inherent property of M2s.

These results are in good agreement with the solid-state NMR studies in micelles, demonstrating that a 25-residue peptide with the sequence of *T. californica* δ-M2 is helical throughout its length, except for a few residues at the N- and C-terminal ends (Opella et al., 1997). Qualitatively similar results were obtained by molecular dynamics calculations of lone M2s (Sankararamakrishnan and Sansom, 1994). In nAChR, the kinks may be stabilized by interactions of M2s with other transmembrane segments and with intrapore waters. Noteworthy is the observation that Ser^8 has conservative neighbors Ile/Val, the bulky β-branched side chains of which should avoid the hydrophilic environment of the pore and hence may cause backbone deformation.

The model of the open channel

The above considerations suggest that M2 helices of nAChR should diverge at the synaptic end of the pore and that intersegment interactions should stabilize the kinks initially proposed by Unwin (1993). In the absence of other transmembrane segments, a five-helix bundle model with the diverging M2s is not expected to correspond even to a local minimum of energy. Therefore, restraints are necessary to keep together the helices diverging from the kinks to the synaptic end of the pore. On the other hand, the cytoplasmic parts of M2s (from the kinks to the N ends) may come in contact with each other. Contacts between blockers and the channel would depend on conformations and orientations of M2s and, hence, on the restraints supporting the diverging parts of M2s. We considered the restraints as additional variables in the search for a model of the pore

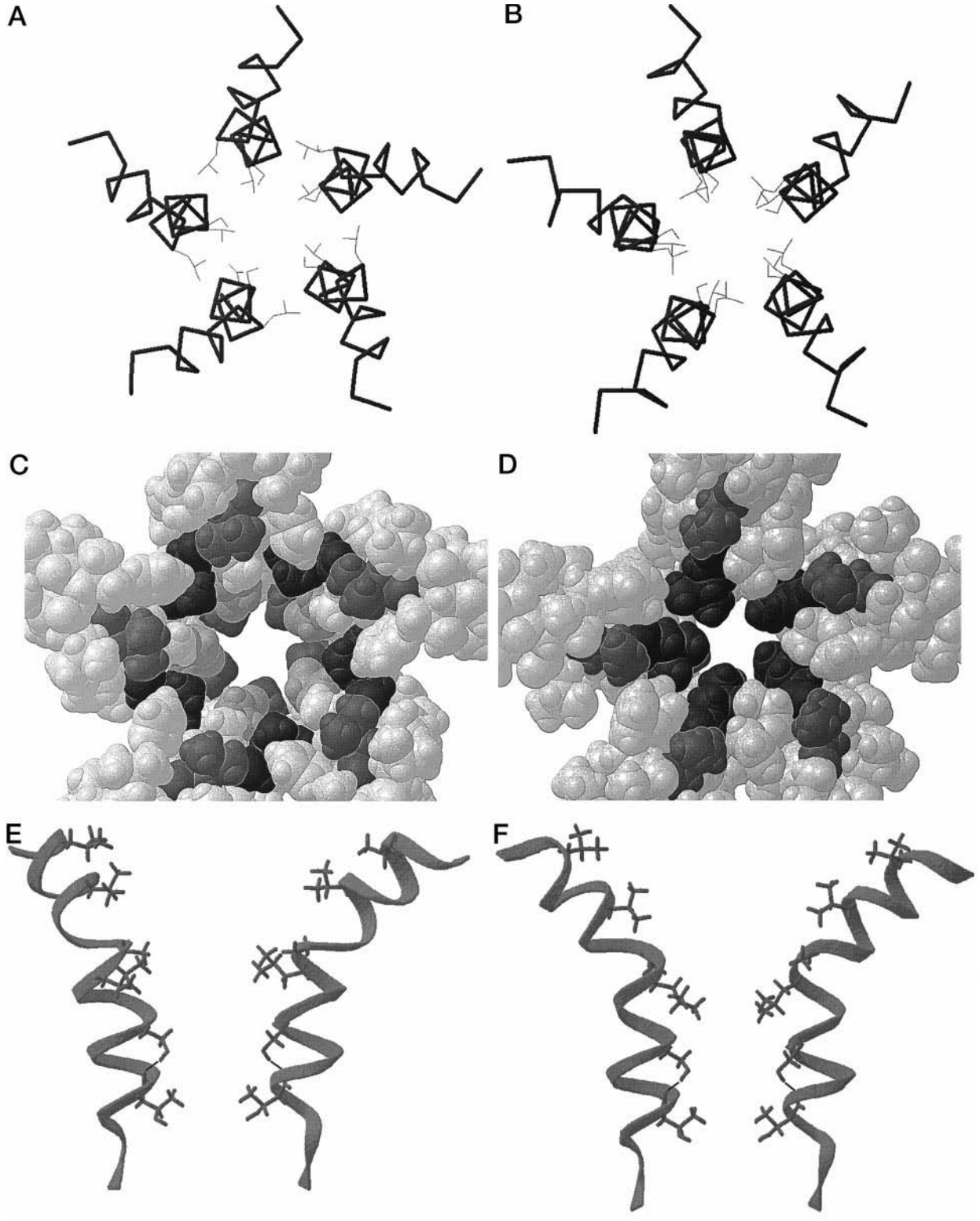

FIGURE 1 C^{α} Tracing (*A, B*), space-filled (*C, D*), and ribbon (*E, F*) presentations of the optimal model of the nAChR channel (MP8) in the open (*A, C, E*) and the closed (*B, D, F*) states viewed from the extracellular (*A–D*) and membrane-exposed (*E, F*) sides. Along with C^{α} tracing, *A* and *B* show side chains of Thr^{4}, Ser^{8}, and Leu^{11} residues as thin lines. In the space-filled representation, Thr^{4} and Val^{15} rings are shown in dark grey, the Ser^{8} ring in light grey, and Leu^{11} in black. In the open state, Thr^{4} and Ser^{8} rings are accessible from the outside. In the closed state, Leu^{11} residues protrude into the pore, making it too narrow for the permeation of hydrated cations. The ribbon diagrams show two nonadjacent M2s with the pore-lining residues (positions 4, 8, 11, 12, 15, and 18) and highlight the intrasegment side chain to main-chain H-bonds.

that would be optimal energetically and agreeable with the available experimental data.

We created 10 models of the pore (designated MP1–MP10) by restraining C^{α} atoms of the pore-facing residues 4, 8, 15, 18, and 19 at various distances from the pore axis (Table 2). The axis was represented by a set of fixed pseudo-atoms (that do not interact with the channel and the blockers) separated from each other by 1 Å. Starting structures were assembled as symmetrical bundles of the straight helices (corresponding to the optimal MECs of the lone M2) with the helical axes parallel to the pore axis. MCM trajectories ($N_u = 500$) were calculated for each model, with the main-chain torsions in the residues 1–8 and 12–21 kept rigid. The obtained MECs with energies below 7 kcal/mol from the apparent global minimum were further minimized, with all of the torsions allowed to vary. Although each MCM trajectory started with the straight helices, the requirements for Thr^4 and Ser^8 to be equally distant from the pore axis and for Val^{15} and Leu^{18} to be increasingly distant from the pore axis yielded kinks in the flexible region Val^9-Ala^{12}.

Models MP2, MP3, and MP5 (Table 2) were rejected after a visual inspection because they had small kinks inconsistent with the requirements for the binding of the blockers. For other models, the energy profiles of the six blockers shown in Table 3 were calculated. A starting point of each profile was obtained by positioning the blocker at the extracellular extension of the pore axis. At each point of the profile, atom N^+ of the blocker (in bisammonium blockers, atom N^+ in the smaller cationic head) was restrained to a pseudo-atom at the given level of the pore axis, and the energy was minimized with M2 positions, orientations, and backbone torsions kept fixed. A realistic model was expected to provide a free access for all of the blockers to the pore, but impose energy barriers of at least 7 kcal/mol that would retard the blockers at the binding sites known from experiments.

Most of the models failed to yield energy profiles satisfying the above requirements. For instance, the profile for CPZ in MP4 showed a high energy barrier at the level of Leu^{11} that would not let CPZ approach the Ser^8 ring. The profile for compound (III) in MP10 did not have a barrier at the Thr^4 ring that would retard the thrimethylammonium head of the blocker. In such a channel, compound (III) would leak through the pore. The profiles for compound (II) in MP1 and MP6 had high barriers at the Ser^8 ring that would not let the trimethylammonium head reach the Thr^4 ring. The best agreement between the calculated energy profiles and the experimental data on the location of the binding sites of the compounds (I)–(VI) was found for MP8. Further refinement of MP8 (see below) decreased its energy without significant changes in the geometry. The C^{α} tracing, space-filled, and ribbon presentations of the refined model MP8 are shown in Fig. 1, *a*, *c*, and *d*, respectively. Some geometrical parameters of model MP8 are given in Table 4.

Sankararamakrishnan et al. (1996) used restraints derived from the electron microscopy data by Unwin (1993, 1995) to create a kinked-helices model of nAChR with a rather wide pore. To account for the experimental data on the permeation of organic cations through the pore and on the blockade of nAChR, the authors suggested that the real dimensions of the pore are smaller because of wall-bound waters. Our model agrees less with the electron microscopy images, but it does not require wall-bound waters to explain the well-known data on channel permeability and blockade. In the electron microscopy image of the open channel, the intracellular parts of M2s slope tangentially to the pore axis by ~45° and form a right-handed barrel. Unwin (1995) noted that the tangential slope of the helices provides a larger exposure of Ser^8 and Thr^4 in the pore. In our model, the requirement for Thr^4 and Ser^8 side chains to face the pore caused a right tangential slope of ~10° in the cytoplasmic parts of M2s. The synaptic parts of M2s in our model have a radial slope of ~40°, which is similar to that observed in the closed channel (Unwin, 1993). Because of this slope, the parts of M2s from the kinks to the C-ends diverge, so that M1s would penetrate partially between

TABLE 2 Models of the pore (MP1–MP10) obtained with restraints (D, Å) between the five C^{α} atoms in the ring of the given residues and the nearest pseudo atom (X) at the pore axis

D(Leu^{18}-X), D(Val^{19}-X)	D(Val^{15}-X)	D(Thr^4-X) = D(Ser^8-X)				
		5.5	5.9	6.2	6.6	6.9
12.5	10.5	MP1	MP2	MP3	MP4	MP5
15.0	12.0	MP6	MP7	MP8	MP9	MP10

TABLE 3 Noncompetitive blockers of nAChR and their binding sites

N	Compound	Binding site	Reference
I	Et_3N^+-$(CH_2)_5$-N^+Et_3	Ser^8	Brovtsyna et al. (1996)
II	Et_3N^+-$(CH_2)_5$-N^+Me_3	Ser^8, Thr^4	Brovtsyna et al. (1996)
III	Me_3N^+-$(CH_2)_5$-N^+Me_3	Ser^8, Thr^4	Brovtsyna et al. (1996)
IV	Me_3N^+-$(CH_2)_5$-N^+H_3	Thr^4	Brovtsyna et al. (1996)
V	QX-222	Ala^{12}, Ser^8	Charnet et al. (1990)
VI	Chlorpromazine	Leu^{11}, Ser^8	Revah et al. (1990)

TABLE 4 Restraints (D) corresponding to the optimal model of the pore and geometrical parameters (R, Z) of the model

Parameter	Residues					
	Thr^4	Ser^8	Leu^{11}	Val^{15}	Leu^{18}	Val^{19}
D*	6.2	6.2	NA	12.0	15.0	15.0
R#	2.2	2.9	4.9	7.1	10.9	11.0
Z§	0	5.8	10.2	17.6	20.1	21.2

* Restraints (see Table 2).
# Distance (Å) between the pore axis' pseudo-atom nearest to the RMS plane drawn via C^{α} atoms of the given residues and the nearest to it point at the van der Waals surface of the ring of the residues.
§ Distance (Å) between the RMS plane drawn via C^{α} atoms of the given residues and the RMS plane drawn via C^{α} atoms of Thr^4 residues.

M2s. Because M1s and M2s span the membrane in opposite directions, only N-parts of M1s may be accessible from the pore. This agrees with the prediction of Furois-Corbin and Pullman (1989) and with the experimental data (DiPaola et al., 1990; Akabas and Karlin, 1995).

Blockers in the pore

The energy-minimized profiles for the blockers (I), (II), and (IV) in model MP8 are given in Fig. 2. The total conformational energy (Fig. 2 *c*) and its electrostatic (Fig. 2 *a*) and nonbonded (Fig. 2 *b*) components are calculated for different positions of the ligands along the pore. The electrostatic profiles for all of the blockers are similar. They are determined by the interactions of Thr^4 and Ser^8 hydroxyls with the positive charge at the blockers' ammonium group. For each of the effective blockers (II), (III), (V), and (VI), the deepest minimum of nonbonded energy (Fig. 2 *b*) coincides with the minimum of electrostatic energy. For the compounds (I) and (IV), the minima of nonbonded and electrostatic energy do not coincide. These compounds are poor blockers of nAChR (Brovtsyna et al., 1996).

An energy-minimized profile strongly depends on the starting structure and, hence, provides only a rough estimate of the interactions between a blocker and the channel. To eliminate the influence of rather arbitrary starting conformations, we calculated MCM-optimized profiles for all of the blockers in MP8. Each profile was obtained by calculating 35 MCM trajectories ($N_u = 100$) for 35 positions of the blocker. The starting point in each trajectory was the MEC obtained in the corresponding position of the energy-minimized profile. In each trajectory, atom N^+ of the blocker was restrained to a pseudo-atom in the pore axis, and conformations and orientations of the blocker and M2s were MCM-optimized. Fig. 3 shows the energy-minimized and MCM-optimized profiles of CPZ in the pore. The MCM optimization yielded a significant decrease in the conformational energy (Fig. 3 *c*) and its electrostatic (Fig. 3 *a*) and nonbonded (Fig. 3 *b*) components as compared to the energy-minimized profile. The wide minimum in the MCM-optimized profile suggests a certain mobility of CPZ in the pore. Both energy-minimized and MCM-optimized profiles have similar coordinates of the nonbonded energy barriers that retard CPZ and other blockers (profiles are not shown) at the corresponding binding sites. The coordinates of these barriers at the energy-minimized profiles were the major criteria for selecting the optimal model MP8. The fact that MCM-optimized profiles yielded similar coordinates of the barriers is evidence of the validity of MP8.

Fig. 4 shows the lowest-energy complexes of the blockers with nAChR that were found in calculations of MCM-optimized energy profiles. The optimal mode of binding of compound (I) shows one of two NEt_3 groups retarded at the Ser^8 ring without reaching the Thr^4 ring (Fig. 4 *a*). This agrees with the prediction by Brovtsyna et al. (1996). The week electrostatic interactions of the blocker with the Ser^4 and Thr^4 rings (Fig. 2 *a*) may explain its low activity. In

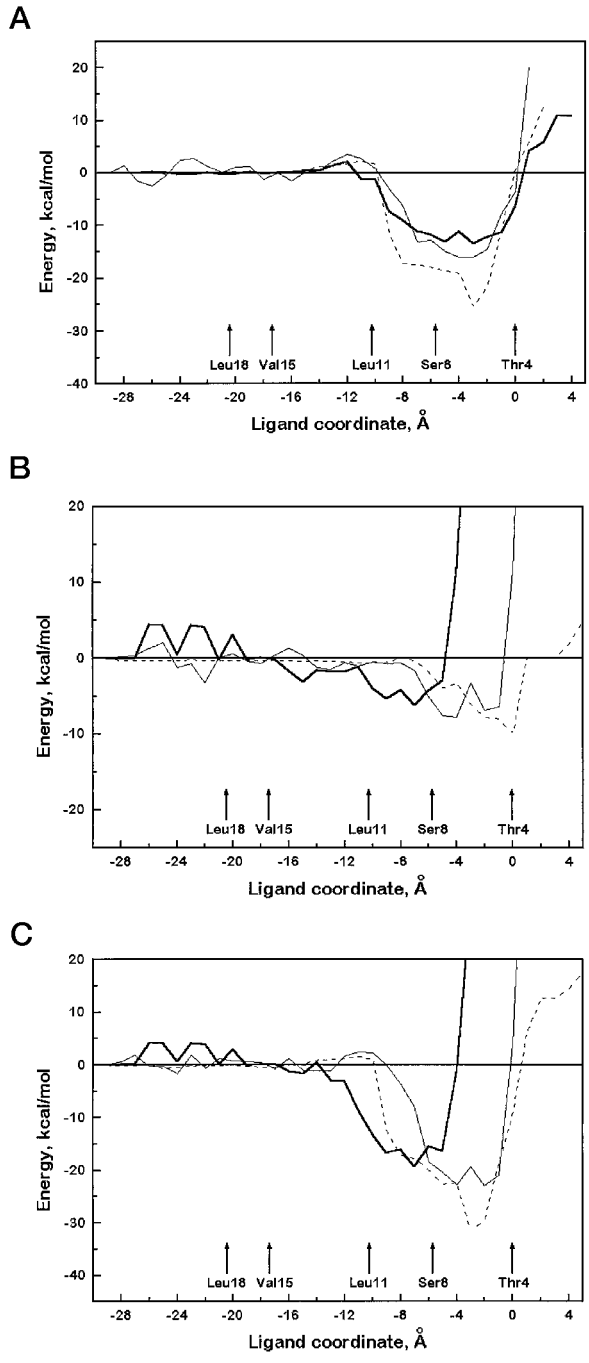

FIGURE 2 Energy-minimized profiles of the compounds I (*bold lines*), II (*thin lines*), and IV (*dashed lines*) in the open-channel model of nAChR (MP8). (*A*) Electrostatic energy. (*B*) Nonbonded energy. (*C*) Total energy. A coordinate of a blocker specifies the position of atom N^+ in the blocker's smaller cationic head relative to the RMS plane drawn via C^α atoms of the Thr^4 ring. The negative coordinates correspond to the extracellular direction. The energies are normalized to be zero at the entry of the pore, where the blockers practically do not interact with the channel. The electrostatic energy profiles for all of the blockers have wide and deep minima between Leu^{11} and Thr^4 rings. The nonbonded energy profiles have relatively shallow minima with the steep energy barriers between Ser^8 and Thr^4 rings. The positions of these barriers correlate with the dimensions of the compounds (the smaller blockers penetrate deeper into the pore). The N^+Et_3 group of compound (I) cannot pass the Ser^8 ring. The N^+Me_3 group of compound (II) meets sterical hindrances at the level of the Thr^4 ring. The ammonium group of compound (IV) can pass through the channel.

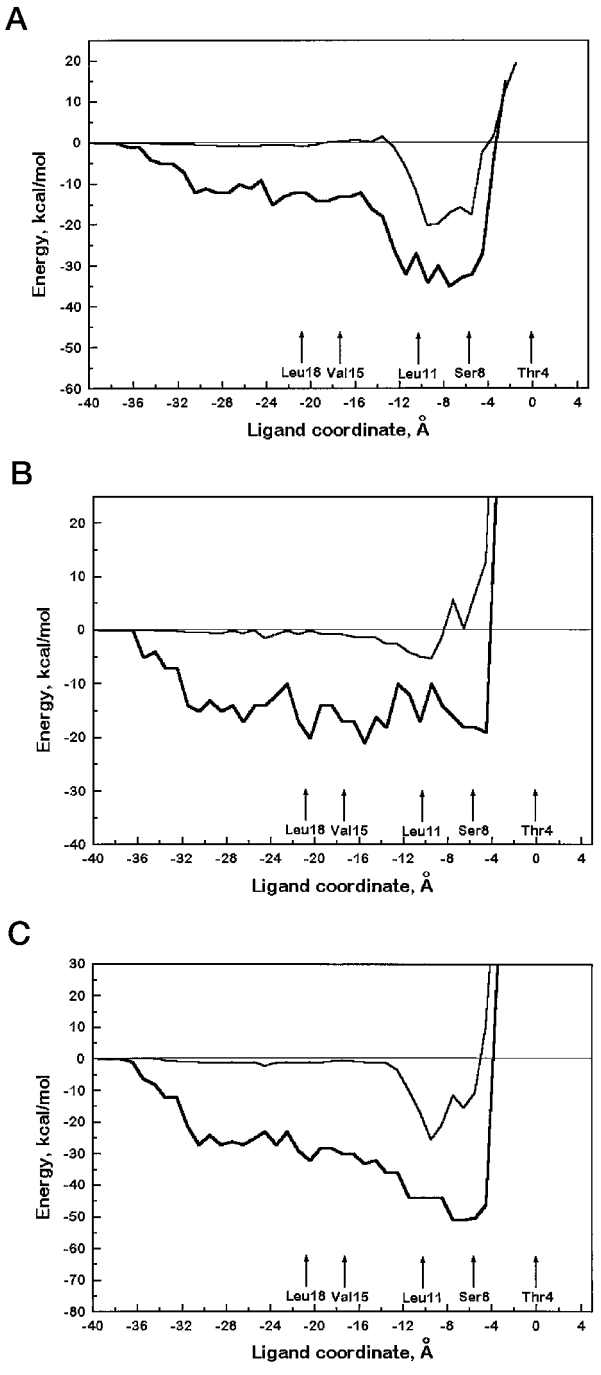

FIGURE 3 Energy-minimized (*thin lines*) and MCM-optimized (*bold lines*) energy profiles of chlorpromazine (CPZ) in the open-channel model of nAChR (MP8) with the fixed backbone torsions. (*A*) Electrostatic energy. (*B*) Nonbonded energy. (*C*) Total energy. A coordinate of CPZ specifies the position of its atom N^+ relative to the RMS plane drawn via C^α atoms of the Thr^4 ring. The negative coordinates correspond to the extracellular direction. The profiles are normalized to have a zero energy at the entry of the pore, where CPZ practically does not interact with the channel.

compound (II), NMe_3 group binds between the Ser^8 and Thr^4 rings, whereas the bulky NEt_3 group interacts effectively with Ala^{12} and Leu^{11} residues (Fig. 4 *b*). This binding mode disagrees with our earlier prediction that the small and the large cationic heads of the compound (II) would interact with the Thr^4 and Ser^8 rings, respectively (Brovtsyna et al., 1996). Our present calculations confirm the prediction by Tikhonov et al. (1996) that the NH_3 group of compound (IV) would pass through the Thr^4 ring. The minima of nonbonded and electrostatic interactions of compound (IV) with MP8 do not coincide with each other. This explains the low activity of compound (IV). Both energy-minimized and MCM-optimized profiles for QX-222 predict that the ligand's NMe_3 group and aromatic moiety bind, respectively, at the Ser^8 ring and the Leu^{11}/Ala^{12} rings (Fig. 4 *c*). Substitution of Ala^{12} by Ser^{12} would weaken the binding of the hydrophobic ring of QX-222. This agrees with the experimental data of Charnet et al. (1990). [H^3]CPZ labels position 8 in five M2s, position 11 in two M2s, and position 4 in only γ-M2 of the *T. californica* nAChR channel (Revah et al., 1990), suggesting an asymmetry of the pore not considered in our model. The optimal binding mode of CPZ (Fig. 4 *d*) shows the phenothiazine moiety interacting with Leu^{11}, Ala^{12}, and carbonyl oxygens of the Ser^8 ring; the amino group of CPZ interacts with the side-chain oxygens of the Ser^8 ring and approaches the Thr^4 ring. Because the photoreactive phenothiazine moiety of CPZ is far from the Thr^4 ring, the model does not explain the labeling of Thr^4 in γ-M2. Another low-populated binding mode of CPZ may exist with the alkylamino chain folded up to let one of the aromatic rings approach Thr^4. An intercalation of the tricyclic moiety of CPZ between M2 segments also cannot be ruled out.

Various noncompetitive blockers of nAChR demonstrate a tissue selectivity. For example, procaine blocks muscle and neuronal nAChRs with different voltage dependencies (Cuevas and Adams, 1994). It is unclear whether the difference is due to peculiarities of the pore-lining residues or of M2 backbone conformations. Mutagenesis experiments may rule out one of these possibilities. For example, if an engineered muscle receptor with the pore-lining residues from a neuronal receptor would mimic the latter by its pharmacological properties, it would indicate that the two receptors have similar backbone conformations of M2s.

In the present model, Ser^8 and Thr^4 hydroxyls form H-bonds with the main-chain carbonyls at the previous helical turns. Hydroxyl oxygens of Thr^4 and Ser^8 protrude into the pore and form two hydrophilic rings important for the permeation of cations and for the binding of the blockers' positively charged groups (note wide minima of electrostatics energy between the Ser^8 and Thr^4 rings, Fig. 2 *a*). The kinks release Ser^8 main-chain oxygens from H-bonds with HN Ala^{12} groups. Lone electron pairs of these oxygens face the pore, forming an additional hydrophilic ring (Fig. 5 *a*) whose location between the wide extracellular part of the channel and the narrow part should be important for the permeation. This may be a "physiological" reason for the kinks.

A model of nAChR is also expected to explain the permeability of the channel for organic cations. Different experiments predict different dimensions of the pore. Dwyer et

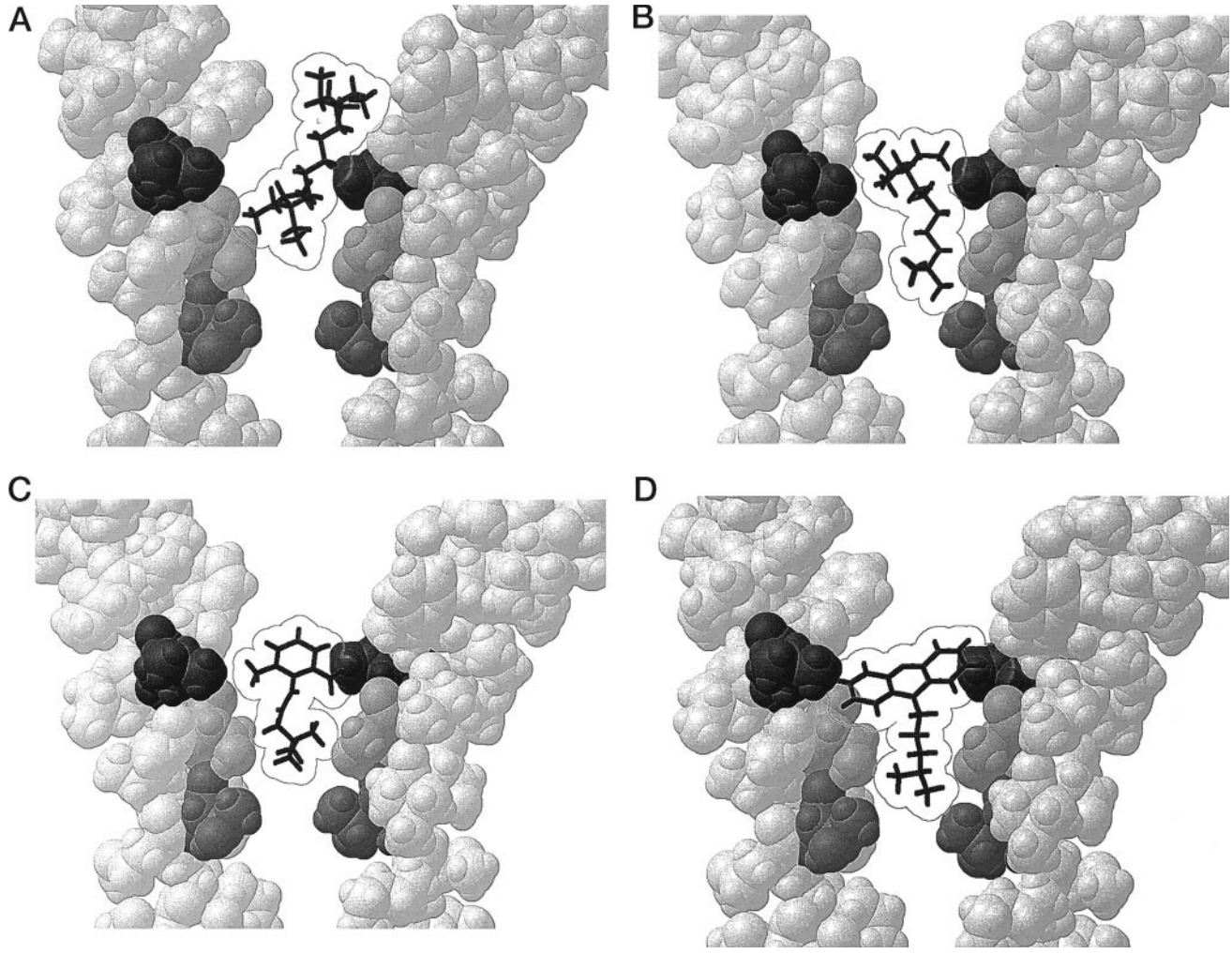

FIGURE 4 Optimal complexes of nAChR with the blockers. Only two nonadjacent M2 segments are shown. The Thr^4 ring is shown in dark grey, the Ser^8 ring in light grey, and Leu^{11} in black. (*A*) A bulky N^+Et_3 group of compound (I) cannot pass the Ser^8 ring and reach the Thr^4 ring. (*B*) Compound (II) binds to the Ser^8 and Thr^4 rings by the N^+Me_3 group, whereas the N^+Et_3 group binds to the Leu^{11} and Ala^{12} rings. (*C*) The aromatic group of QX-222 interacts with Leu^{11} and Ala^{12} rings, and the N^+Me_3 group with the Ser^8 ring, in agreement with mutagenesis experiments by Charnet et al. (1990). (*D*) The phenothiazine moiety of the CPZ molecule interacts with Leu^{11} and Ala^{12} rings, whereas the cationic head interacts with the Ser^8 and Thr^4 rings, in agreement with affinity labeling experiments by Revah et al. (1990).

al. (1980) approximated the minimal cross-sectional dimensions of the open pore in the frog muscle receptor by a rectangle of 6.5 × 6.5 Å. Cohen et al. (1992) estimated the pore diameter to be as large as 8.4 Å. Nutter and Adams (1995) predicted the minimal diameter of the neuronal receptor to be 7.6 Å. Taking into account the conformational flexibility of the organic cations and measuring the minimum silhouettes of their high-populated conformations, Brovtsyna et al. (1996) estimated the minimum dimensions of the neuronal receptor to be 5.5 × 6.4 Å. The pore dimensions in our present model are close to those predicted by Dwyer et al. (1980) and Brovtsyna et al. (1996). The essential difference in the predicted dimensions of the pore may be due to the peculiarities of the receptor subtypes studied. It should be noted, however, that a circle or a rectangle is a rough approximation for the lumen cross section, and the channel walls as well as organic ions are conformationally flexible. Calculation of MCM-optimized profiles for permeating organic cations may help correlate their chemical structure with the permeation properties. This interesting problem was not addressed in the present study.

Channel gating

Mutation of Leu^{11} residues affects desensitization and gating of nAChR (Revah et al., 1991; Filatov and White, 1995; Labarca et al., 1995). A possible mechanism of the gating assumes notable rotations of entire M2s, with Leu^{11} residues exposed in the pore, precluding the permeation of the hydrated cations and the kinked regions acting as molecular swivels (Unwin, 1995). Indeed, noncompetitive antagonist 3-(trifluoromethyl)-3-(m-[^{125}I]iodophenyl)diazirine (TID) labels Val^{16} and Leu^{11} rings in the closed channel and Val^6,

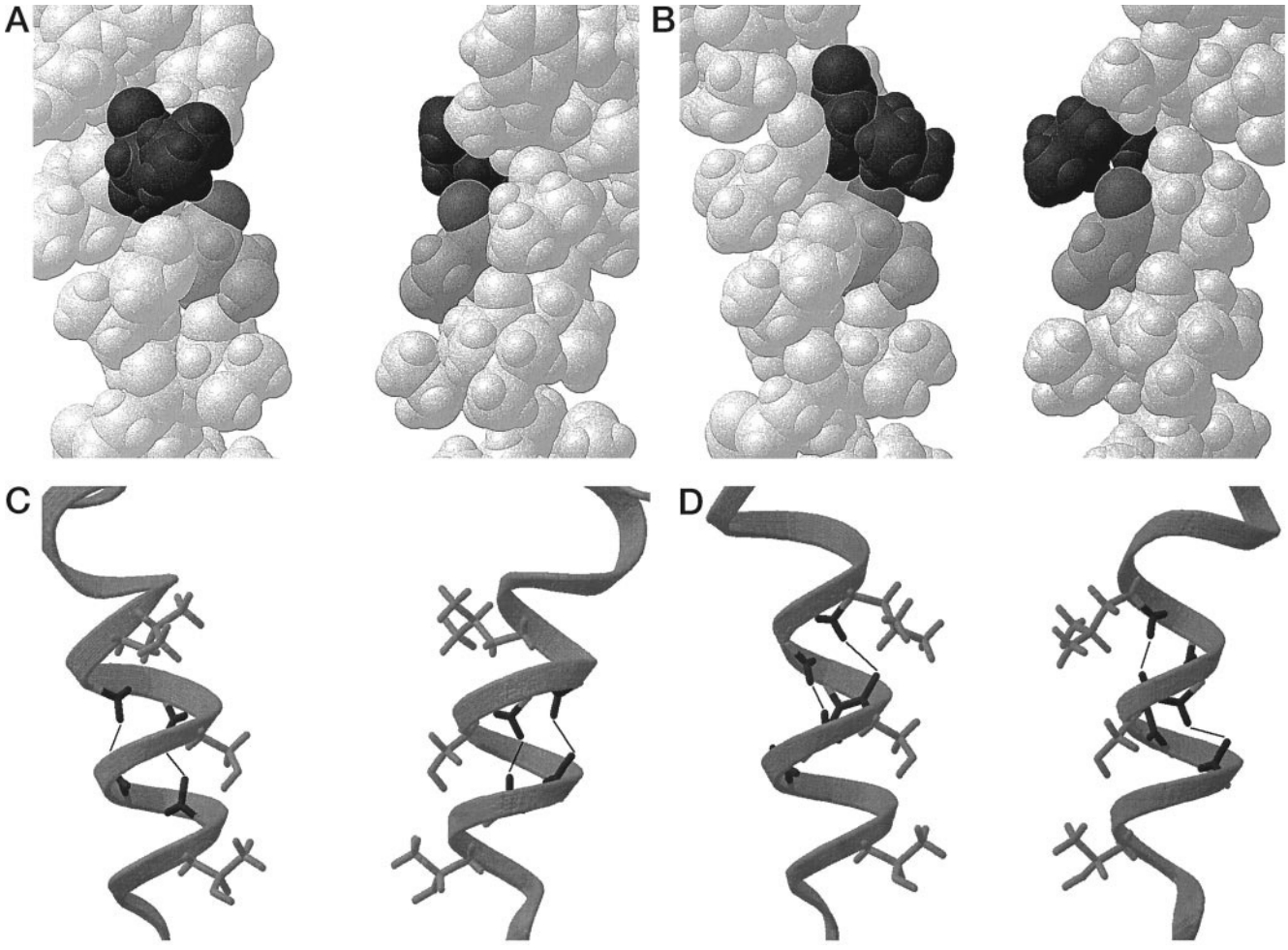

FIGURE 5 Space-filled (*A, B*) and ribbon (*C, D*) presentations of the kinked region of nAChR pore in the open (*A, C*) and closed (*B, D*) conformations. In the open state, main-chain oxygens (*dark grey*) of Ser^{8} residues (*light grey*) protrude into the pore and form a polar ring that may be important for the permeation of cations. In the closed state, this ring is shielded by the hydrophobic side chain of Leu^{11} (*black*). The ribbon diagrams show the side chains of Thr^{4}, Ser^{8}, and Leu^{11} residues and highlight H-bonds that stabilize the kinks.

Leu^{11}, Thr^{4}, and Ser^{8} rings in the open channel (White et al., 1991; Cohen et al., 1992). However, cysteine scanning did not reveal an essential difference in the accessibility of individual residues of M2s in the open and closed states of the channel (Akabas et al., 1994; Akabas and Karlin, 1995). If pore-facing hydrophobic residues form a constriction whose dimensions are comparable with those of hydrated cations, even minor conformational changes in the residues may dramatically affect the permeation, thus causing an elementary phase of the gating (Zhorov and Ananthanarayanan, 1996). Leu^{11} residues are located at the kinks, where the split system of H-bonds provides a high flexibility to the backbones. Some conformations of the flexible backbones may represent the closed states of the channel, whereas other conformations may correspond to the open states, suggesting that rotations of entire M2s may not be necessary for channel gating.

To explore this possibility, we calculated a long MCM trajectory ($N_u = 2000$) of the five-helix bundle. Positions and orientations of M2s and the torsions of the residues 1–8 and 13–21 were kept fixed, the torsions of the residues 9–12 being randomized. The search yielded 45 different structures with energies up to 7 kcal/mol from the apparent global minimum. In these structures, the kinked regions of M2s had a split network of α-helical H-bonds. However, each kinked region was stabilized by at least one intrasegment H-bond. We found conformers with the α-helical H-bonds Ser^{6}···Leu^{10} and Ile^{7}···Leu^{11} (Fig. 5 *c*), as well as conformers with the 3_{10}-helical H-bonds Ser^{6}···Val^{9} and Ile^{7}···Leu^{10} (Fig. 5 *d*). In the conformers with the α-helical H-bonds, Ala^{12} faced the pore, suggesting that such conformers represent the pore-opening states of M2s. In the conformers with the 3_{10}-helical H-bonds, Leu^{11} faced the pore, suggesting that these conformers may represent the pore-closing states of M2s. The 45 collected structures of the five-helix bundle comprised 225 different conformers of M2s, among which 52 conformers corresponded to the pore-closing states.

At the next stage, we selected two structures of the bundle corresponding to the open and to the closed channel, and

energy-minimized them, with all of the torsions allowed to vary. The obtained models are shown in Fig. 1 and the torsions of one of the M2s in Fig. 6, and energies are given in Table 5. The structure shown in Fig. 1, *a*, *c*, *e*, represents the open channel with Ala^{12} facing the pore. The structure shown in Fig. 1, *b*, *d*, *f*, represents the closed channel with Leu^{11} residues protruding into the pore and diminishing its radius up to 1.75 Å. This pore is too narrow to let through the hydrated Na^+, whose radius is 2.4 Å (Moore, 1972).

In the closed channel, we also found a candidate for another 3_{10}-helical H-bond, Leu^{11}_NH···O_Ser^8, with a distance of 2.54 Å (Fig. 5 *d*). Our model with the rigid valence geometry did not allow further approach by Leu^{11}_NH of O_Ser^8. However, this H-bond may occur in the real channels. The hydrophobic side chain of Leu^{11} would stabilize this H-bond by protecting it from the intrapore waters (Fig. 5 *b*), whereas in M2 with Ser^{11}, the waters would destabilize it and hence the closed state of the channel. Indeed, Leu^{11} to Ser^{11} mutation does destabilize the closed state of nAChR (Labarca et al., 1995). Thus the gating of the nAChR channel may be due to conformational changes in the short flexible chains (involving Leu^{11} residues) that connect more stable α-helical parts of M2s. This model does not require energetically expensive rearrangements of the transmembrane segments; the latter may be necessary to transfer the channel to the long-lasting desensitized states (Feltz and Trautmann, 1982).

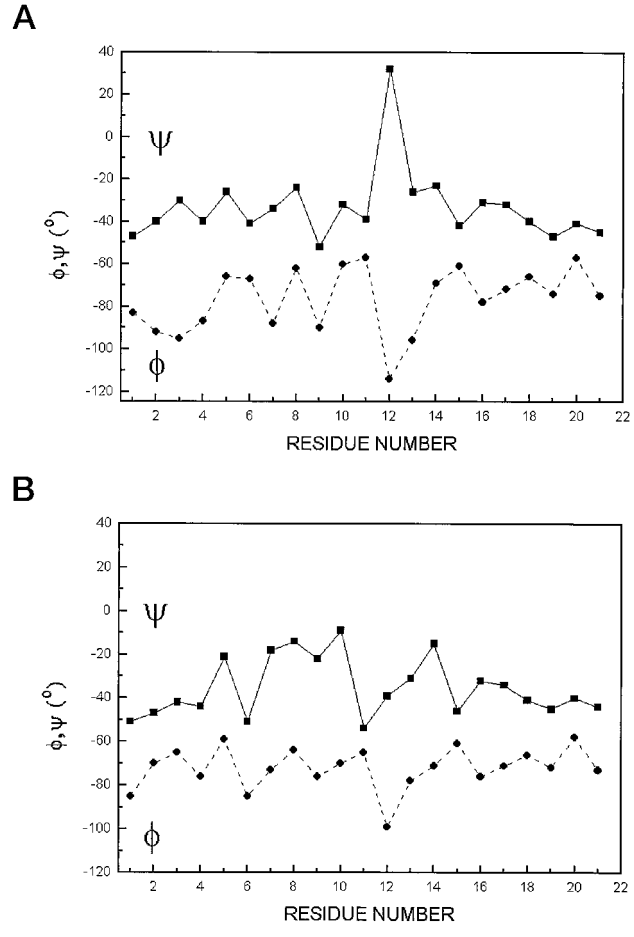

FIGURE 6 Backbone torsions versus residue numbers of M2 in the pore-opening (*A*) and pore-closing (*B*) conformations.

TABLE 5 Energy (kcal/mol) of the models of the open and the closed states of nAChR

Energy component	Closed state	Open state
Electrostatic	−180.4	−147.7
Nonbonded	−577.9	−599.4
H-bonds	−179.8	−157.9
Torsional	142.2	129.0
Constrains	2.9	1.5
Total energy	−793.1	−774.5

At the synaptic end of the pore, M1s may fill the space between the diverging M2s. Cysteine mutants in the N end part of M1 are labeled by sulfhydryl reagents, with accessibility of residues highly dependent on the presence of acetylcholine (Akabas and Karlin, 1995). M1s are close to the acetylcholine recognition site of nAChR (Devillers-Thiery et al., 1993) and may link this site with the effector part of the gating mechanism. For example, agonist-induced conformational changes in M1s may shift an equilibrium between the open and the closed states in the kinked regions of M2s. This mechanism would explain why mutations in the inner, intermediate (Glu^1) and Thr^4 rings affect mainly the ion permeation via the channel (Imoto et al., 1988, 1991; Konno et al., 1991; Villarroel et al., 1991). These rings are at the cytoplasmic part of the pore, where M2s come in contact with each other, so that their conformations do not depend on the channel's gating. Contrarily, in the synaptic part, M2s interact with M1s that may transmit the signal from the acetylcholine recognition site to the gate. Indeed, mutations at this region affect the gating and desensitization of nAChR (Revah et al., 1991; Labarca et al., 1995).

Essentially different roles were proposed for Leu^{11} residues: occlusion of the pore during desensitization (Revah et al., 1991; Bertrand et al., 1993), stabilization of the closed state of the channel by interacting with each other (Unwin, 1993), governing channel gating (Labarca et al., 1995), and setting the mean open time through interactions with other regions of the channel rather than forming the gate itself (Filatov and White, 1995). Our model visualizes the former two roles. Below we propose a possible explanation of the experiments that question the gating role of Leu^{11} residues.

Based on the finding that Leu^{11} substitution by Thr in only one of the five M2s stabilized the open state of the channel and assuming that the remaining four Leu^{11} residues would still effectively occlude the pore, Filatov and White (1995) concluded that Leu^{11} residues do not form the gate. However, a permeation of a hydrated cation via a ring of hydrophobic residues may be highly sensitive, even to small changes in the dimensions of the ring (Zhorov and Ananthanarayanan, 1996). Cations should permeate via the open hydrophobic gate with the water entourage. If the dimensions of the open gate match those of the hydrated

cation, exposing only one Leu^{11} residue to the agonist-bound channel would transfer it in a nonconducting state. In our model, conformational transitions in each M2 are independent. Brief channel closings during a burst can be explained as stochastic transitions of one of M2s to the "closed" conformation. Consecutive mutations of each Leu^{11} by Ser or Thr may progressively decrease the probability of the nonconducting states of the agonist-bound channel and, hence, increase the probability of the open states. If only a portion of the agonist-bound channels are open simultaneously, these mutations should also increase the population of the open channels, i.e., their apparent affinity to agonists. These effects were observed in the experiments by Labarca et al. (1995) and Filatov and White (1995). These experiments also demonstrated a gating in the channels with all five Leu^{11} residues substituted by Ser or Thr, suggesting that residues at other positions may protrude into the pore and block the ion permeation.

Akabas et al. (1994) demonstrated that the closed cannel is more accessible to a sulfhydryl reagent ethylammonium derivative of methanethiosulfonate (MTSEA) than the open channel (see Table 1). Based on these data and on the fact that the replacement of the extracellular Na^+ by MTSEA did not increase the leak current, Akabas et al. (1994) suggested that the gate of the channel is at least as cytoplasmic as Glu^1. However, MTSEA may pass the closed Leu^{11} gate in the deprotonated state. In this state, the amino group is poorly hydrated, and the minimum silhouette of MTSEA is rather small.

Our interpretations of the experiments on the channel gating do not rule out the original interpretations. Various conducting and nonconducting states of nAChR may be possible, and our model may visualize only some of the possibilities. Further studies are necessary to prove or disprove the proposed mechanism of the gating.

CONCLUDING REMARKS

The model of the nAChR pore composed of the consensus M2s explained general properties of the nAChR pore and peculiarities of its blockade by various compounds. Like any atomic-scale computational model, our model presents details with a resolution not achievable by contemporary experimental methods. Of course, not all of these details are equally reliable. A single model cannot accommodate all of the available experimental data with their original interpretations. Thus our model reproduces kinks in M2s observed in electron cryomicroscopy studies, but it is not consistent with the large diameter of the pore implied by the same experiments. Our model supports the idea that Leu^{11} residues are directly involved in the channel gating, but it is inconsistent with other possible interpretations of mutagenesis experiments involving Leu^{11}. We have proposed alternative interpretations that may be tested in further experiments. For example, Leu^{11} to Ile or Val substitutions may affect the channel gating, particularly equilibrium between the conducting and nonconducting states of agonist-activated channels.

Present calculations ignored other transmembrane segments, intrapore waters, and entropy contributions to the free energy. Considering these and other factors should improve the capacity of the models to explain the existing experimental data and make it possible to design new experiments.

We are thankful to L. G. Magazanik for reading the manuscript. This work was supported by grant 96-04-50610 to BSZ from the Russian Foundation for Basic Research. DBT acknowledges support from grant 94-04-48619 for which L. G. Magazanik is the grant recipient.

REFERENCES

Adams, P. R. 1977. Voltage jump analysis of procaine action at frog end-plate. *J. Physiol. (Lond.).* 268:291–318.

Aguayo, L. G., and E. X. Albuquerque. 1986. Effects of phencyclidine and its analogs on the end-plate current of the neuromuscular junction. *J. Pharmacol. Exp. Ther.* 239:15–24.

Akabas, M. H., and A. Karlin. 1995. Identification of acetylcholine receptor channel-lining residues in the M1 segment of the alpha-subunit. *Biochemistry.* 34:12496–12500.

Akabas, M. H., C. Kauffmann, P. Archdeacon, and A. Karlin. 1994. Identification of acetylcholine receptor channel-lining residues in the entire M2 segment of the alpha-subunit. *Neuron.* 13:919–927.

Amador, M., and J. A. Dani. 1991. MK-801 inhibition of nicotinic acetylcholine receptor channel. *Synapse.* 7:207–215.

Antonov, S. M., J. W. Johnson, N. Ya. Lukomskaya, N. N. Potapyeva, V. E. Gmiro, and L. G. Magazanik. 1995. Novel adamantane derivatives act as blockers of open ligand-gated channels and as anticonvulsants. *Mol. Pharmacol.* 47:558–567.

Baenziger, J. E., and N. Methot. 1995. Fourier transform infrared and hydrogen/deuterium exchange reveal an exchange-resistant core of α-helical peptide hydrogens in the nicotinic acetylcholine receptor. *J. Biol. Chem.* 270:29129–29137.

Bechinger, B. K. Y., L. E. Chirlian, J. Gesell, J. M. Neumann, M. Montal, J. Tomich, M. Zasloff, and S. J. Opela. 1991. Orientations of amphipathic helical peptides in membrane bilayers determined by solid-state NMR spectroscopy. *J. Biomol. NMR.* 1:167–173.

Benoit, P., and J. P. Changeux. 1993. Voltage dependencies of the effects of chlorpromazine on the nicotinic receptor channel from mouse muscle sell line Sol8. *Neurosci. Lett.* 160:81–84.

Bertrand, D., J. L. Galzi, A. Devillers-Thiery, S. Bertrand, and J. P. Changeux. 1993. Mutations at two distinct sites within the channel domain M2 alter calcium permeability of neuronal alpha7 nicotinic receptor. *Proc. Natl. Acad. Sci. USA.* 90:6971–6975.

Bolin, J. T., D. J. Filman, D. A. Matthews, R. C. Hamlin, and J. Kraut. 1982. Crystal structure of *Escherichia coli* and *Lactobacillus casei* dihydrofolate reductase refined at 1.7 Å resolution. *J. Biol. Chem.* 257:13650–13662.

Brooks, C. L., B. M. Pettitt, and M. Karplus. 1985. Structural and energetic effects of truncating long ranged interactions in ionic polar fluids. *J. Chem. Phys.* 83:5897–5908.

Brovtsyna, N. B., D. B. Tikhonov, O. B. Gorbunova, V. E. Gmiro, S. E. Serduk, N. Ya. Lukomskaya, L. G. Magazanik, and B. S. Zhorov. 1996. Architecture of the neuronal nicotinic acetylcholine receptor ion channel at the binding site of bis-ammonium blockers. *J. Membr. Biol.* 152: 77–87.

Changeux, J. P., J. L. Galzi, A. Devillers-Thiery, and D. Bertrand. 1992. The functional architecture of the acetylcholine nicotinic receptor explored by affinity labelling and site-directed mutagenesis. *Q. Rev. Biophys.* 25:395–432.

Charnet, P., C. Labarca, R. J. Leonard, N. J. Vogelaar, L. Czyzyk, A. Gouin, N. Davidson, and H. A. Lester. 1990. An open channel blocker

interacts with adjacent turns of alpha-helices in the nicotinic acetylcholine receptor. *Neuron.* 4:87–95.

Cohen, B. N., C. Labarca, N. Davidson, and H. A. Lester. 1992. Mutations in M2 alter the selectivity of the mouse nicotinic acetylcholine receptor for organic and alkali metal cations. *J. Gen. Physiol.* 100:373–400.

Cuevas, J., and D. J. Adams. 1994. Local anaesthetics blockade of neuronal nicotinic ACh receptor-channels in rat parasympathetic ganglion cells. *Br. J. Pharmacol.* 111:663–672.

Devillers-Thiery, A., J. L. Galzi, J. L. Eisele, S. Bertrand, D. Bertrand, and J. P. Changeux. 1993. Functional architecture of the nicotinic acetylcholine receptor: a prototype of ligand-gated ion channels. *J. Membr. Biol.* 136:97–112.

DiPaola, M., P. N. Kao, and A. Karlin. 1990. Mapping the alpha-subunit site photolabelled by the noncompetitive inhibitor quinacrine azide in the active state of the nicotinic acetylcholine receptor. *J. Biol. Chem.* 265:11017–11029.

Dwyer, T. M., D. J. Adams, and B. Hille. 1980. The permeability of the endplate channel to organic cations in frog muscle. *J. Gen. Physiol.* 75:469–492.

Eisenman, G., A. Villarroel, M. Montal, and O. Alvarez. 1990. Energy profiles for ion permeation in pentameric protein channels: from viruses to receptor channels. *In* Progress in Cell Research, Vol. 1. J. M. Ritchie, P. J. Magistrelli, and L. Bolis, editors. Elsevier Science Publishers, Amsterdam. 195–211.

Feltz, A., and A. Trautmann. 1982. Desensitization at the frog neuromuscular junction: a biphasic process. *J. Physiol. (Lond.).* 322:257–272.

Filatov, G. N., and M. M. White. 1995. The role of conserved leucines in the M2 domain of the acetylcholine-receptor in channel gating. *Mol. Pharmacol.* 48:379–384.

Furois-Corbin, S., and A. Pullman. 1989. A possible model for the inner wall of the acetylcholine receptor channel. *Biochim. Biophys. Acta.* 984:339–350.

Galzi, J. L., and J. P. Changeux. 1994. Neurotransmitter-gated ion channels as unconventional allosteric proteins. *Curr. Opin. Struct. Biol.* 4:554–565.

Galzi, J. L., and J. P. Changeux. 1995. Neuronal nicotinic receptors: molecular organisation and regulations. *Neuropharmacology.* 34: 563–582.

Hille, B. 1992. Ionic Channels of Excitable Membranes, 2nd Ed. Sinauer Associates, Sunderland, MA.

Hucho, F., U. Gorne-Tschelnokow, and A. Strecker. 1994. Beta-structure in the membrane-spanning part of the nicotinic acetylcholine receptor (or how helical are transmembrane helices?). *Trends Neurosci.* 19: 383–387.

Hucho, F., and R. Hilgenfeld. 1989. The selectivity filter of a ligand-gated ion channel. *FEBS Lett.* 257:17–23.

Hucho, F., W. Oberthur, and F. Lottspeich. 1986. The ion channel of the nicotinic acetylcholine receptor is formed by the homologous helices MII of the receptor subunits. *FEBS Lett.* 205:137–142.

Imoto, K., C. Busch, B. Sakmann, M. Mishina, T. Konno, J. Nakai, H. Buyo, Y. Mori, K. Kukuda, and S. Numa. 1988. Rings of negatively charged amino acids determine the acetylcholine receptor channel conductance. *Nature.* 335:645–648.

Imoto, K., T. Konno, J. Nakai, F. Wang, M. Mishina, and S. Numa. 1991. A ring of uncharged polar amino acids as a component of channel constriction in the nicotinic acetylcholine receptor. *FEBS Lett.* 289: 193–200.

Konno, T., C. Busch, E. Von Kitzing, K. Imoto, F. Wang, J. Nakai, M. Mishina, S. Numa, and B. Sakmann. 1991. Rings of anionic amino acids as structural determinants of ion selectivity in the acetylcholine receptor channel. *Proc. R. Soc. Lond. B.* 244:69–79.

Labarca, C., M. W. Nowak, H. Zhang, L. Tang, P. Deshpande, and H. A. Lester. 1995. Channel gating governed symmetrically by conserved leucine residues in the M2 domain of nicotinic receptors. *Nature.* 376: 514–516.

Large, W. A., and J. A. Sim. 1986. A comparison between mechanisms of action of different nicotinic blocking agents on rat submandibular ganglia. *Br. J. Pharmacol.* 89:583–592.

Le Novere, N., and J. P. Changeux. 1995. Molecular evolution of the nicotinic acetylcholine receptor: an example of multigene family in excitable cells. *J. Mol. Evol.* 40:155–172.

Leonard, R. J., C. G. Labarca, P. Charnet, N. Davidson, and H. A. Lester. 1988. Evidence that the M2 membrane-spanning region lines the ion channel pore of the nicotinic receptor. *Science.* 242:1578–1581.

Lester, H. A. 1992. The permeation pathway of neurotransmitter-gated ion channels. *Annu. Rev. Biophys. Biomol. Struct.* 21:267–292.

Levitt, M. 1978. Conformational preferences of amino acids in global proteins. *Biochemistry.* 17:4277–4284.

Li, Z., and H. A. Scheraga. 1988. Structure and free energy of complex thermodynamic systems. *J. Mol. Struct.* 179:333–352.

Malashkevich, V. N., R. A. Kammerer, V. P. Efimov, T. Schulthess, and J. Engel. 1996. The crystal structure of a five-stranded coiled coil in COMP: a prototype ion channel? *Science.* 274:761–765.

Momany, F. A., R. F. McGuire, A. W. Burgess, and H. A. Scheraga. 1975. Energy parameters in polypeptides. VII. Geometric parameters, partial atomic charges, nonbonded interactions, hydrogen bond interactions, and intrinsic torsional potentials of the naturally occurring amino acids. *J. Phys. Chem.* 79:2361–2381.

Moore, W. J. 1972. Physical Chemistry. Longman, London.

Neher, E., and J. H. Steinbach. 1978. Local anaesthetic transiently block currents through single acetylcholine-receptor channels. *J. Physiol. (Lond.).* 277:153–176.

Nemethy, G., M. S. Pottle, and H. A. Scheraga. 1983. Energy parameters in polypeptides. 9. Updating of geometrical parameters, nonbonded interactions, and hydrogen bond interactions for the naturally occurring amino acids. *J. Phys. Chem.* 87:1883–1887.

Nutter, T. J., and D. J. Adams. 1995. Monovalent and divalent cation permeability and block of neuronal nicotinic receptor channels in rat parasympathetic ganglia. *J. Gen. Physiol.* 105:701–723.

Oblatt-Montal, M., L. Buhler, T. Iwamoto, J. M. Tomich, and M. Montal. 1993a. Synthetic peptides and four-helix bundle proteins as model systems for the pore-forming structure of channel proteins: transmembrane segment M2 of the nicotinic cholinergic receptor channel is a key pore-lining structure. *J. Biol. Chem.* 268:14601–14607.

Oblatt-Montal, M., T. Iwamoto, J. M. Tomich, and M. Montal. 1993b. Design, synthesis and functional characterization of a pentameric channel protein that mimics the presumed pore structure of the nicotinic cholinergic receptor. *FEBS Lett.* 320:261–266.

Oiki, S., W. Danho, V. Madison, and M. Montal. 1988. M2 delta, a candidate for the structure lining the ionic channel of the nicotinic cholinergic receptor. *Proc. Natl. Acad. Sci. USA.* 85:8703–8707.

Oiki, S., V. Madison, and M. Montal. 1990. Bundles of amphipathic transmembrane alpha-helices as a structural motif for ion-conducting channel proteins: studies on sodium channels and acetylcholine receptors. *Proteins Struct. Funct. Genet.* 8:226–236.

Ortels, M. O., and G. G. Lunt. 1996. A mixed helix-beta-sheet model of the transmembrane region of the nicotinic acetylcholine receptor. *Protein Eng.* 9:51–59.

Opella, S. J., J. Gasell, A. P. Valente, F. M. Marassi, M. Oblatt-Montal, W. Sun, A. Ferrer-Montiel, and M. Montal. 1997. Structural studies of the pore-lining segments of neurotransmitter-gated channel. *CHEMTRACTS Biochem. Mol. Biol.* 10:153–174.

Papke, R. L., and R. E. Oswald. 1989. Mechanisms of noncompetitive inhibition of acetylcholine-induced single-channel currents. *J. Gen. Physiol.* 93:785–811.

Revah, F., D. Bertrand, J. L. Galzi, A. Devillers-Thiery, C. Mulle, N. Hussy, S. Bertrand, M. Ballivet, and J. P. Changeux. 1991. Mutations in the channel domain alter desensitization of a neuronal nicotinic receptor. *Nature.* 353:846–849.

Revah, F., J. L. Galzi, J. Giraudat, P. Y Haumont, F. Lederer, and J. P. Changeux. 1990. The noncompetitive blocker [^{3}H]chlorpromazine labels three amino acids of the acetylcholine receptor gamma subunit: implication for the alpha-helical organization of regions MII and for the structure of the ion channel. *Proc. Natl. Acad. Sci. USA.* 87:4675–4679.

Sands, S. B., and M. E. Barish. 1991. Calcium permeability of neuronal nicotinic channels in PC12 cells. *Brain Res.* 560:38–42.

Sankararamakrishnan, R., C. Adcock, and M. S. P. Sansom. 1996. The pore domain of the nicotinic acetylcholine receptor: molecular modelling, pore dimensions, and electrostatics. *Biophys. J.* 71:1659–1671.

Sankararamakrishnan, R., and M. S. P. Sansom. 1994. Kinked structure of isolated nicotinic receptor M2 helices: a molecular dynamics study. *Biopolymers.* 34:1647–1657.

Tikhonov, D. B., N. N. Potapyeva, V. E. Gmiro, B. S. Zhorov, and L. G. Magazanik. 1996. A proposed binding mechanism of pentamethylene-bisammonium derivatives to the muscle nicotinic acetylcholine receptor channel. *Biol. Membr.* 13:185–195.

Unwin, N. 1993. Nicotinic acetylcholine receptor at 9 Å resolution. *J. Mol. Biol.* 229:1101–1124.

Unwin, N. 1995. Acetylcholine receptor channel imaged in the open state. *Nature.* 373:37–43.

Unwin, N. 1996. Projection structure of the nicotinic acetylcholine receptor: distinct conformations of the alpha subunits. *J. Mol. Biol.* 257:586–596.

Vasquez, M., G. Nemethy, and H. A. Scheraga. 1983. Computed conformational states of the 20 naturally occurring amino acids and of the prototype residue α-aminobutyric acid. *Macromolecules.* 16:1043–1049.

Verino, S., M. Amador, C. W. Luetje, J. Patrick, and J. A. Dani. 1992. Calcium modulation and high calcium permeability of neuronal nicotinic acetylcholine receptor. *Neuron.* 8:127–134.

Villarroel, A., S. Herlitze, M. Koenen, and B. Sakmann. 1991. Location of a threonine residue in the alpha-subunit M2 transmembrane segment that determines the ion flow through the acetylcholine receptor channel. *Proc. R. Soc. Lond. B.* 243:69–74.

Villarroel, A., and B. Sakmann. 1992. Threonine in the selectivity filter of the acetylcholine receptor channel. *Biophys. J.* 62:196–205.

von Kitzing, E. 1995. Structure modelling of the acetylcholine receptor channel, and related ligand gated channels. *In* Modelling of Biomolecular Structures and Mechanisms. A. Pullman, J. Jortner, and B. Pullman, editors. Kluwer Academic Publishers, Dordrecht, the Netherlands. 39–57.

White, B. H., S. Howard, S. G. Cohen, and G. B. Cohen. 1991. The hydrophobic photoreagent 3-(trifluoromethyl)-3-m-([^{125}I]iodophenyl)-diazirine is a novel noncompetitive antagonist of the nicotinic acetylcholine receptor. *J. Biol. Chem.* 266:21595–21607.

Zhorov, B. S. 1981. Vector method for calculating derivatives of energy of atom-atom interactions of complex molecules according to generalized coordinates. *J. Struct. Chem.* 22:4–8.

Zhorov, B. S. 1983. Vector method for calculating derivatives of the energy deformation of valence angles and torsion energy of complex molecules according to generalized coordinates. *J. Struct. Chem.* 23: 649–655.

Zhorov, B. S. 1993. Comparison of lowest-energy conformations of dimethylcurine and methoxyverapamil: evidence of ternary association of calcium channel, Ca^{2+}, and calcium entry blockers. *J. Membr. Biol.* 135:119–127.

Zhorov, B. S., and V. S. Ananthanarayanan. 1996. Structural model of synthetic Ca^{2+} channel with bound Ca^{2+} ions and dihydropyridine ligand. *Biophys. J.* 70:22–37.

Zhorov, B. S., N. B. Brovtsyna, V. E. Gmiro, N. Ya. Lukomskaya, S. E. Serduk, N. N. Potapyeva, L. G. Magazanik, D. E. Kurenniy, and V. I. Skok. 1991. Dimensions of the ion channel in neuronal nicotinic acetylcholine receptor as estimated from analysis of conformation-activity relationships of open-channel blocking drug. *J. Membr. Biol.* 121: 119–132.